STScI | SPACE TELESCOPE SCIENCE INSTITUTE

Instrument Science Report WFC3 2023-06

The WFC3/UVIS G280 Grism Sky

A. Pagul, R. Ryan, B. Kuhn, D. Som

September 18, 2023

Abstract

We have constructed the first sky images for the WFC3/UVIS G280 grism from both the calibrated, flat-fielded individual FLT exposures, as well as their corresponding CTE-corrected FLC frames using public on-orbit science exposures retrieved from the Mikulski Archive for Space Telescopes (MAST). We characterize the sources of stray light present in the G280 science frames, and provide guidance for minimizing stray light depending on the levels of precision needed for observers' science cases. We search for the potential presence of multiple spectral components—however we determine that a single component should be sufficient to model the scattered light present in the G280 science exposures. We find the stray light scatters in an expected pattern for the WFC3/UVIS detector and we do not find additional spectral components from OII emission in Earth's atmosphere. After processing data using our sky model with `HSTaXe`*, we reduce the median of the background distribution for our test cases to one compatible with 0.0 electrons per second (e^-/s), providing bounds for cases with both low- and high-levels of scattered light, i.e. from 0.0494 to 0.0025 e^-/s and 0.3747 to 0.0002 e^-/s, respectively. We also show that our sky model reduces the spatial variations across the two UVIS chips, where the change in background depends on the pixel's chip position. We present the procedure used for our analysis and for the generation of the sky frames. We provide existing resources for WFC3 spectral analysis and applying these calibration frames with* `HSTaXe`*. In the future, we plan to examine changes in the spatial trends of the sky with time and if possible, provide a means to predict background levels given observing conditions necessary for specific science cases.*

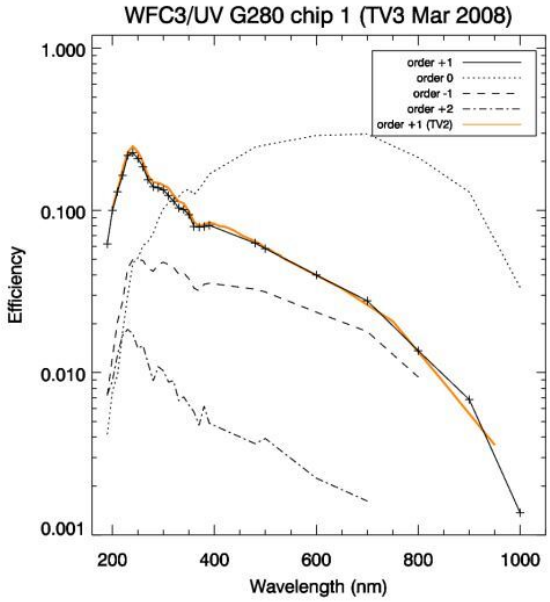

Figure 1: Efficiency curve of the G280 grism as presented in Kuntschner et al. 2009.

Introduction

The G280 grism is one of three grisms mounted on the Wide Field Camera 3 (WFC3), and the only grism available in the UVIS channel (WFC3 Instrument Handbook; Dressel and Marinelli 2023). Its throughput spans a wide wavelength range (200 - 1000 nm), with peak throughput in the 200-400 nm range (Figure 1 from Kuntschner et al. 2009 – Figure 1). The high throughput that G280 affords blueward of 800 nm makes it an attractive instrument mode to use for various scientific studies, including the measurement of exoplanet atmospheres (Wakeford et al. 2020, Lewis et al. 2020). Minimizing the detector systematics and sky contributions is necessary to improve spectral extractions for these science cases.

In this ISR, we analyze different sources that can contribute to increasing the background electrons (e^-) and introducing spurious structures. After careful analysis and characterization we construct a G280 sky reference file to efficiently remove these backgrounds. In doing so, we also analyze sky contributions from different components, including the zodiacal light, diffuse galactic light, and other stray light originating from sunlight, moonlight, and Earthshine. Similar studies (Caddy, Spitler, and Ellis 2022, Carleton et al. 2022, O'Brien et al. 2023) have been conducted in the context of characterizing sky and extragalactic background light observed by low Earth telescopes (specifically the Hubble Space Telescope). Furthermore, similar analyses and techniques have been developed in previous works that constructed sky calibration frames for the WFC3/IR G102 and G141 grism (Kümmel et al. 2011,Brammer, Ryan, and Pirzkal 2015). We build on these previous works by analyzing similar characteristics in the WFC3/UVIS G280 filter. The optical bench for the WFC3/UVIS camera is set up such that all stray light scatters on the CCD, with a flare pattern characteristic of internal reflection. Nevertheless, we check for other spectral components that might be present in the G280 background, including the oxygen emission lines at small Earth limb

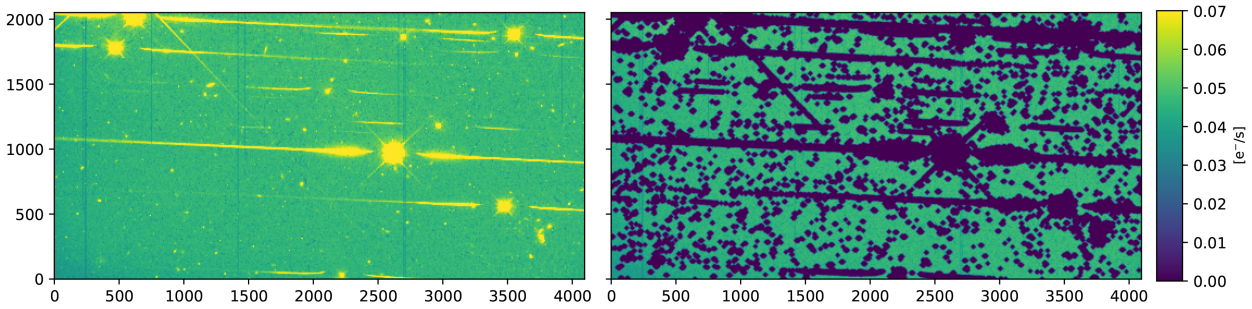

Figure 2: Left: Example image (`icwz44qyq` from GO 12524; PI Quimby) used in the analysis. Right: Example segmentation map used to mask sources.

angles.

In this work, we provide not only global statistics, but we also empirically generate calibration frames to describe the spatial distribution of dispersed background light that is present in the WFC3/UVIS G280 grism observations.

Analysis

Dataset

For this analysis, we retrieve all G280 frames that are publicly available on MAST as of July 2023, downloading both the FLT and the corresponding CTE-corrected FLC frames. In total, we analyze 506 full-frame images for this work. We also consider including the FLT sub-frames in our analysis; however, while this addition would improve the statistics in the construction of our sky images, these subframes are mostly calibration images of GRW+70, and the systematics introduced by this bright calibration star, as well as the lack of spatial coverage of the full chip, does not improve the results.

Source Masking

Each G280 frame retrieved from MAST are multi-extension FITS files, which contain the science exposure in e^-, the error map in e^-, and a data quality (DQ) mask containing information about bad pixels. In pre-processing the images, we first divide by the exposure time to ensure consistent e^-/s units across all frames. We then use the DQ array to mask the appropriate bad pixels (DQ>0). We run `Source Extractor` (Bertin and Arnouts 1996) on the science frame and use inverse variance weighting derived from the error map. We use a convolution kernel designed to detect the extended grism trace and dispersion (Brammer, Pirzkal, et al. 2014).

One of the `Source Extractor` outputs is a segmentation map, which assigns a region in the image to each object that has been detected in the frame. We use the `scipy` submodule `ndimage.binary_dilation`[1] where the structuring element is a square with connectivity

[1] `ndimage.binary_dilation` API

equal to 1. We use 20 iterations to dilate the segments and use this modified segmentation map in order to mask the extended profiles of each source. An example of the results of this masking procedure is shown in Figure 2.

Background Characterization

In the process of generating the sky, we identify the main contributors to scattered light by correlating different variables, including the zodiacal light (which we will refer to as zodi), Moon angle, and Earth limb angle, with the median background levels and its spatial structure.

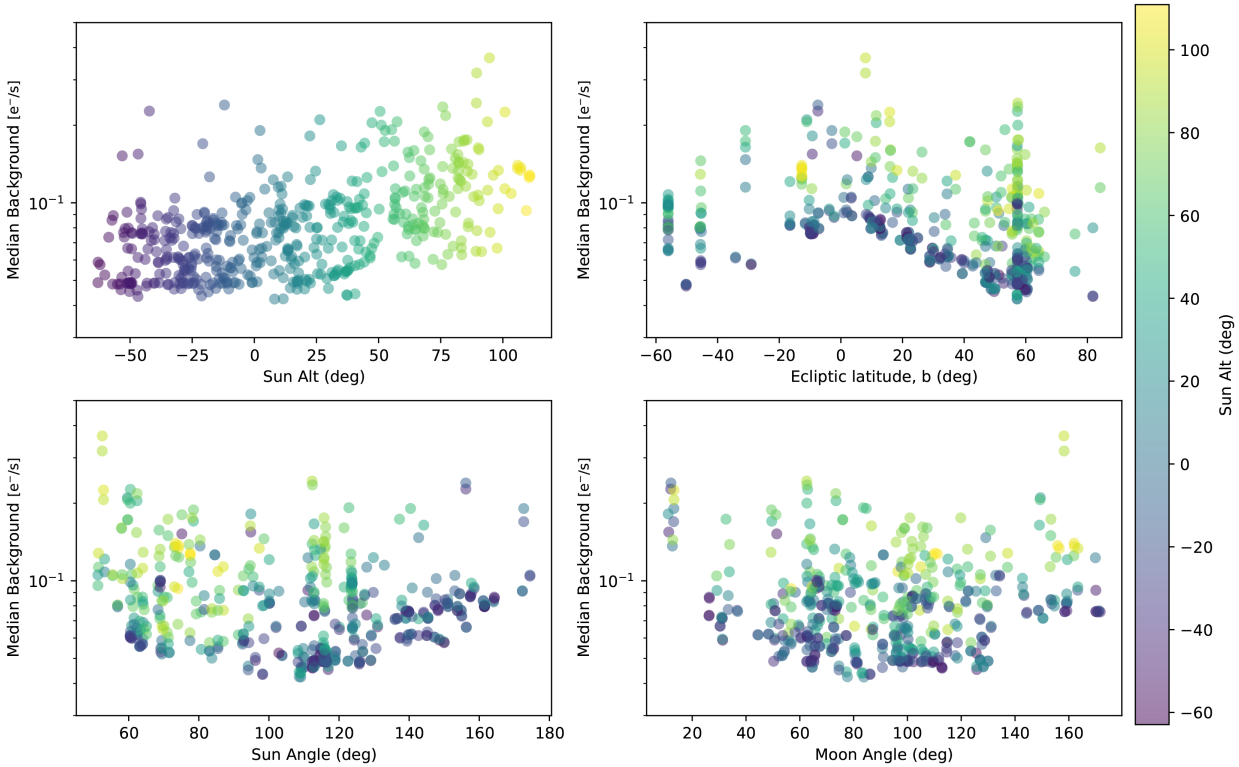

Figure 3: Top left: Median background measured as a function of Sun Altitude. Top right: Median background as a function of ecliptic latitude. Bottom left: Median background as a function of Sun Angle. Bottom right: Median background as a function of Moon Angle. All data-points are color-coded by Sun Altitude.

Figure 3 shows median background levels of all 506 full-frame G280 exposures as a function of various observing parameters. In the top left corner, the median background is plotted versus the Sun altitude. The median background is stable when observations are taken in Earth's shadow, and starts increasing as the Sun rises above the daytime Earth (Sun alt >0, denoted with green and yellow points). In the top right corner, we plot the median background versus the ecliptic latitude. We note the typical shape associated with the zodiacal background, with values rising as absolute ecliptic latitude approaches 0 degrees. Note that for observations taken in the daytime Earth, we find a large envelope above the isolated

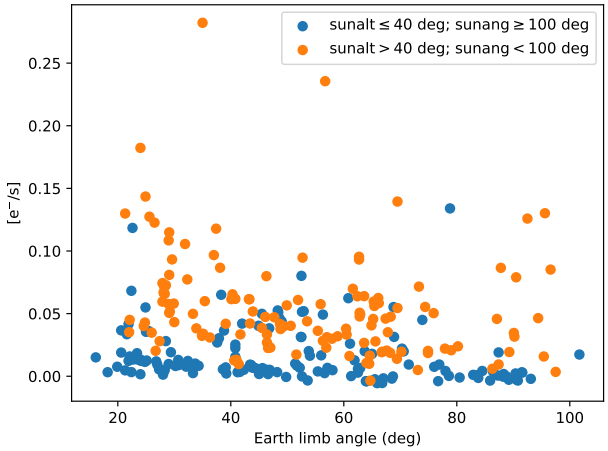

Figure 4: After correcting for the zodi component, we split the daytime Earth sample into two subsets, one with sun altitude $\leq$ 40 degrees and sun angle $\geq$ 100 degrees (blue points) and one with sun altitude $>$ 40 degrees and sun angle $<$ 100 degrees (orange points), and note a bifurcation in background values between the blue and orange points at Earth limb angles $\lesssim$ 55 degrees.

zodi contribution. In the lower left panel, we plot the median background versus the Sun angle, or angular separation between the target and the Sun. A u-shape trend emerges here even though we expect the background to decrease with increasing Sun angle. This is due to multiple effects, specifically, we found the higher points at high Sun angles correspond to zodiacal light (|ecliptic latitude| $<$ 20 deg). In the lower right panel, we plot median background versus the Moon angle (angle between the target, or HST boresight, and the Moon).

After He 10830Å emission was detected in the WFC3/IR G102 and G141 grism (Brammer, Pirzkal, et al. 2014), we check for the presence of potential emission line features, such as OII, in the G280 data. While we do not see any statistically significant emission line features, we note that in daytime Earth, smaller Earth limb angles, high sun altitudes, and smaller sun angles, correspond to higher background values (Figure 4, orange points).

We first isolate the zodiacal light contribution by minimizing other contaminating sources, that is, we consider those frames that are taken in the Earth's shadow (Sun altitude $<$ 0 deg), outside of the Galactic plane (|galactic latitude| $>$ 20 deg), and with a large angular separation between the source and the Moon/Sun (Moon angle $>$ 20 deg; Sun angle $>$ 75 deg).

We note that while each of the individual components from our background characterization contributes to the total measurement of stray light due to the features of the optical bench for the UVIS CCD, the light scatters similarly in all cases. Nevertheless, in separating out sources of scattered light, we select "zodi-only" frames by minimizing contributions from other sources of scattered light for our analysis.

Generating the sky frames

A total of 170 frames remain after selecting for the zodi-only. We divide each frame by its median background, normalizing the frame to a median of 1. We then generate an array of size $N_{\rm frames} \times 2051 \times 4096$ for each chip and use the `astropy` submodule `stats.sigma_clipped_stats`[2] to median stack the frames along the $N_{\rm frames}$ dimension. We note that some pixels will not have any data in them due to masking from either spectra or the DQ flags and we fill these pixels with a value of 1.

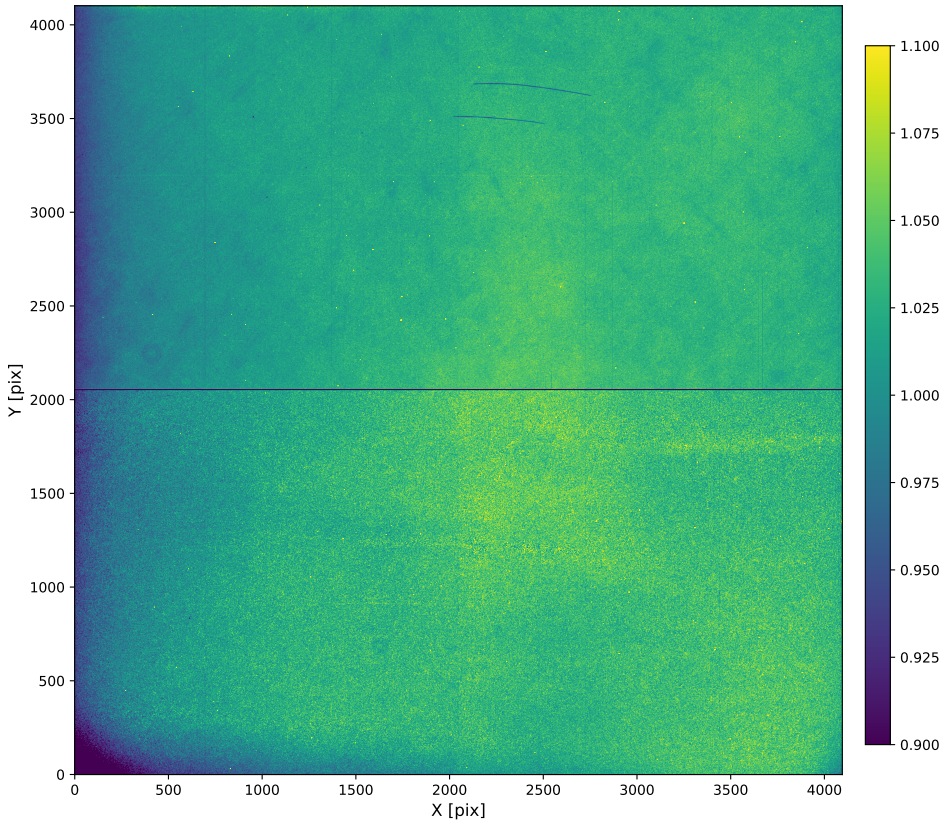

Figure 5: G280 FLC sky

The resulting zodi model for both UVIS1 and UVIS2 is shown in Figure 5. We note both the flare and cross-hatch patterns, which Mack 2016 found to be due to internal reflection and changing detector temperatures, respectively. These features are also present in the UVIS reference flat fields (Sabbi 2008), including the overlapping broadband flat field images, such as the direct image filter, F300X, as well as F350LP.

[2] `stats.sigma_clipped_stats` API

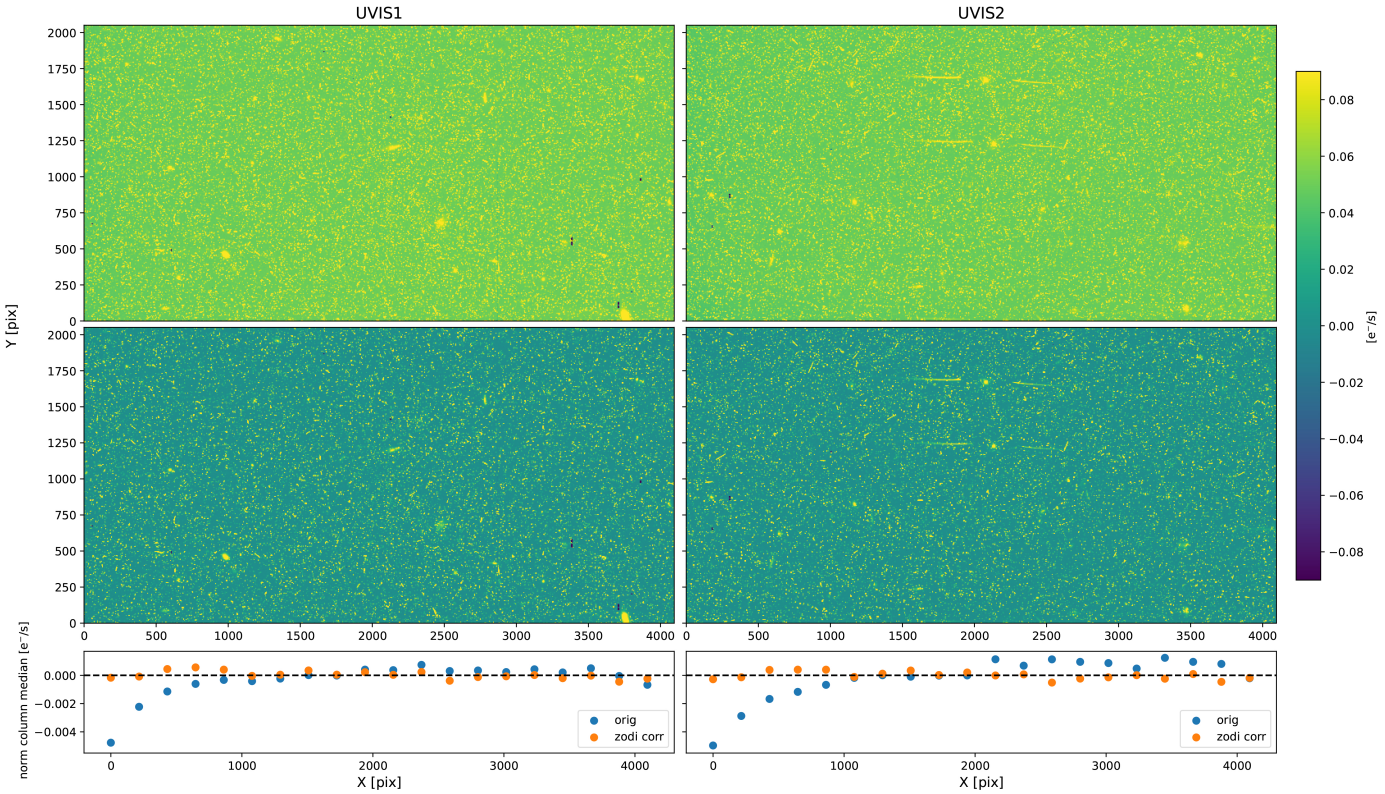

Figure 6: Examples of sky reduction for UVIS1 (left) and UVIS2 (right) (`icwz50hbq` from GO 14127; PI Fumagalli). The top row corresponds to the original frame; the middle row corresponds to the zodi-subtracted frame; the bottom row corresponds to the column medians across the x-axis normalized to 0.

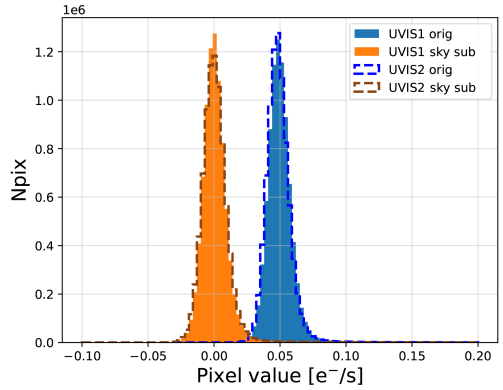

(a) Pixel value distribution histograms of the original and corrected science frames for UVIS1 and UVIS2 from Figure 6. Note how the zodi-corrected (orange) histogram is centered around 0, providing a sanity check that the global correction is correctly applied.

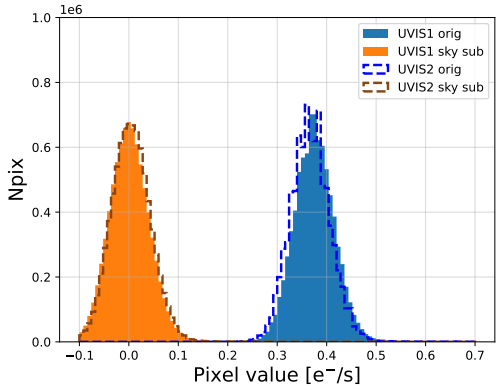

(b) Pixel value distribution histograms of the original and corrected science frames for UVIS1 and UVIS2 from the highest e$^-$/s datapoint, `ib3d34a6q` from GO 11594; PI O'Meara. Here the original distribution is also shifted and centered at 0.

Figure 7: Pixel value distributions for low- (left; 7a) and high-background (right; 7b) frames before and after sky subtraction.

Applications to science imaging

We apply the zodi model from Figure 5 using `HSTaXe` (Sosey et al. 2023), software that was developed for grism spectral extraction. We set the `backims` keyword to denote the path to our sky file and set the `backgr` keyword to `True` to tell `HSTaXe` to apply the background subtraction. Since our sky is normalized to 1, `HSTaXe` fits the appropriate coefficient by which to multiply the calibration image to then subtract from the science image. An example sky subtraction for UVIS1 and UVIS2 is shown in Figure 6, where the top row panels show the original frames (UVIS1 on the left and UVIS2 on the right), the middle row shows the sky-corrected image for both chips, and the bottom row represents the column median versus x-pixels. In the plot, the blue points correspond to the original image and the orange points to the sky-corrected image. We shift the medians to 0 so that both distributions are easily comparable. We note that after applying the sky, the spatial variation across each chip is reduced by a factor dependent on chip and position on that chip. The largest improvement in this example is seen on the left quarter of both UVIS1 and UVIS2 (removing up to ∼0.005 e$^-$/s of zodi contribution) and on the right half of UVIS (∼0.002 e$^-$/s of zodi).

We also plot histograms of the global pixel distribution, comparing the original pixel distribution to the sky-corrected one. Figure 7a shows the pixel values for a low-background image are shifted with a center from 0.0494 to 0.0002 e$^-$/s; figure 7b shows the pixel values for our highest-background image in e$^-$/s, where the histogram is shifted from 0.3747 to 0.0025 e$^-$/s. These two examples provide bounds for the background ranges of existing images and verify that our background is removed sufficiently well in both low- and high-background regimes.

We also demonstrate the effect of applying the sky on spectra. Using the UVIS full frame

grism extraction notebook to run `HSTaXe`, we extract the spectra of a source in exposure `icwz50hbq`. Figure 8 shows the result of the spectral extraction before (blue curve) and after (orange curve) sky subtraction. As expected, the background-corrected spectral flux decreases, and this decrease is non-uniform due to the spatial variation of the sky.

Summary

We have constructed a sky image for the WFC3/UVIS G280 grism using data that is publicly available on MAST as of July 2023. The sky image was generated by median-stacking frames selected to include the zodi-only contribution. We mask both the objects and bad pixels before stacking the frames. Given the discovery of the atmospheric Helium II line in the WFC3/IR grism sky frames, we check for spectral features, specifically in daytime Earth and at small Earth limb angles, potentially corresponding to dispersion due to OII lines excited in the upper atmosphere. However, due to the instrument design and baffling, as well as the relative weakness of the OII lines at these wavelengths, we do not find any additional residuals in our image stacks.

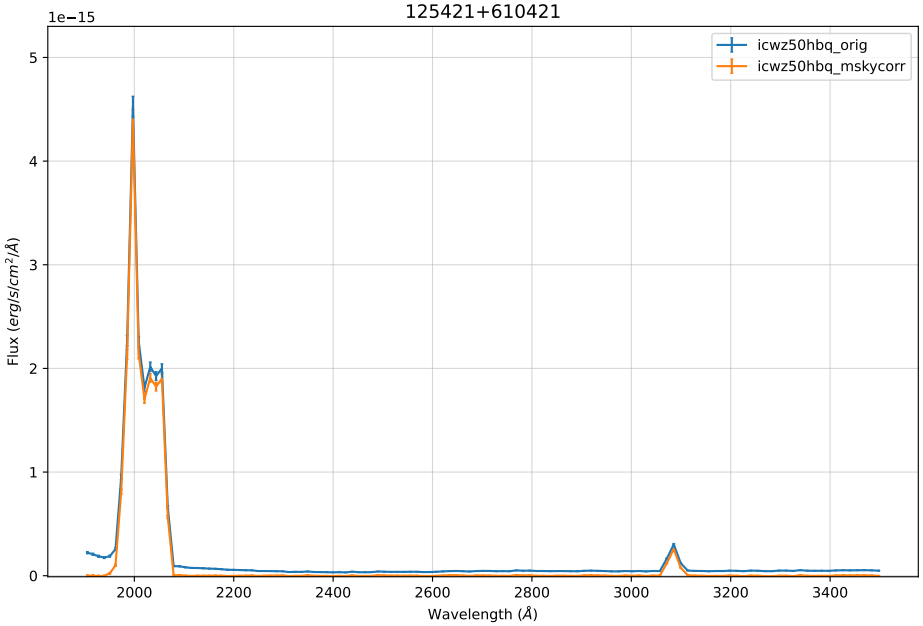

Figure 8: Example spectral extraction for exposure `icwz50hbq`. The spectrum extracted from the background-corrected science exposure (orange) is successfully shifted closer to zero than the uncorrected exposure (blue). The magnitude of the correction varies across wavelength as expected due to the spatial variation of the background.

After applying our sky frames on a sample set of G280 exposures, we find the sky subtraction successfully shifts the center of the distribution of background pixel values to 0 e^-/s and flattens spatial variations in the background and extracted `HSTaXe` spectra.

We provide a G280 sky image for each UVIS chip, and for both FLC and FLT calibration frames on the STScI Grism Resources page. These calibration frames can be used as input in the `HSTaXe` spectral extraction software, where the observer can set background subtraction to `True` using the `backgr` keyword and define the image path using the `backims` keyword. For a tutorial on extracting spectra from G280 grism frames with `HSTaXe`, please see the G280 extraction cookbook.

Acknowledgements

The authors wish to thank Sylvia Baggett and Jennifer Mack for their extensive guidance and leadership on this work. We would also like to thank the HST Grism Working Group who facilitated an environment of open discussion and idea-generation to make this work possible. Finally, we would like to thank Joel Green, Sylvia Baggett, and Mariarosa Marinelli for their helpful comments, which improved the quality of this work.

References

Bertin, E. and S. Arnouts (June 1996). "SExtractor: Software for source extraction." In: 117, pp. 393–404. DOI: 10.1051/aas:1996164.

Brammer, G., N. Pirzkal, et al. (Apr. 2014). *Time-varying Excess Earth-glow Backgrounds in the WFC3/IR Channel*. Instrument Science Report WFC3 2014-03, 14 pages.

Brammer, G., R. Ryan, and N. Pirzkal (Nov. 2015). *Source-dependent master sky images for the WFC3/IR grisms*. Instrument Science Report WFC3 2015-17, 18 pages.

Caddy, Sarah E., Lee R. Spitler, and Simon C. Ellis (Aug. 2022). "Toward a Data-driven Model of the Sky from Low Earth Orbit as Observed by the Hubble Space Telescope". In: 164.2, 52, p. 52. DOI: 10.3847/1538-3881/ac76c2. arXiv: 2205.16002 [astro-ph.IM].

Carleton, Timothy et al. (Nov. 2022). "SKYSURF: Constraints on Zodiacal Light and Extragalactic Background Light through Panchromatic HST All-sky Surface-brightness Measurements: II. First Limits on Diffuse Light at 1.25, 1.4, and 1.6 μm". In: 164.5, 170, p. 170. DOI: 10.3847/1538-3881/ac8d02. arXiv: 2205.06347 [astro-ph.CO].

Dressel, Linda and Mariarosa Marinelli (2023). "WFC3 Instrument Handbook for Cycle 31 v. 15.0". In: *WFC3 Instrument Handbook for Cycle 31 v. 15.0*. Vol. 15, p. 15.

Kümmel, M. et al. (Jan. 2011). *Master sky images for the WFC3 G102 and G141 grisms*. ST-ECF Instrument Science Report WFC3-2011-01, 10 pages.

Kuntschner, H. et al. (Jan. 2009). *The ground calibrations of the WFC3/UVIS G280 grism*. ST-ECF Instrument Science Report WFC3 2009-01, 23 pages.

Lewis, N. K. et al. (Oct. 2020). "Into the UV: The Atmosphere of the Hot Jupiter HAT-P-41b Revealed". In: 902.1, L19, p. L19. DOI: 10.3847/2041-8213/abb77f. arXiv: 2010.08551 [astro-ph.EP].

Mack, J. (Mar. 2016). *UVIS 2.0: Ultraviolet Flats*. Instrument Science Report WFC3 2016-05, 30 pages.

O'Brien, Rosalia et al. (June 2023). "SKYSURF-4: Panchromatic Hubble Space Telescope All-Sky Surface-brightness Measurement Methods and Results". In: 165.6, 237, p. 237. DOI: 10.3847/1538-3881/acccee. arXiv: 2210.08010 [astro-ph.IM].

Sabbi, E. (June 2008). *UVIS CASTLE Photometric Filter Flat Field Atlas*. Instrument Science Report WFC3 2008-012, 13 pages.

Sosey, Megan et al. (July 2023). *spacetelescope/hstaxe: v1.0.5*. Version v1.0.5. DOI: 10.5281/zenodo.8136948. URL: https://doi.org/10.5281/zenodo.8136948.

Wakeford, H. R. et al. (May 2020). "Into the UV: A Precise Transmission Spectrum of HAT-P-41b Using Hubble's WFC3/UVIS G280 Grism". In: 159.5, 204, p. 204. DOI: 10.3847/1538-3881/ab7b78. arXiv: 2003.00536 [astro-ph.EP].